DEM-CFD-based simulation and optimization of a combined pneumatic-centrifugal wheat seed-metering device

Duanxu Ma, Song Shi, Hui Li, Guojian Wei, Jilei Zhou, Yupeng Shi, Hu Liu*

(*Shandong Academy of Agricultural Sciences, Jinan 250100, China*)

Abstract: Pneumatic wheat seed-metering device often has a poor seed-filling state under the high-speed working condition, which adversely affects precision seeding. This paper describes a wheat seed-metering device that employs a combined mechanical–pneumatic seed-filling method. The orifice structure and seed-filling space at the nozzle are optimized to improve the seed-filling efficiency and seed-carrying stability. The working process of the wheat seed-metering device was analyzed, the principles of the seed-filling and seed-cleaning processes were elucidated, the factors influencing the seed-filling performance and seed-carrying stability were investigated, and the discrete element method–computational fluid dynamics (DEM-CFD) simulation method was employed to simulate the working process. The nozzle-orifice diameter, seed-filling-space angle, and rotation speed were determined as the simulation influence factors, and the trends of the nozzle void fraction, resistance to clearing, and initial dropping position were analyzed from a microscopic scale. On a macroscopic scale, the seed-leakage rate, reseeding rate, and grain-spacing qualification rate as performance-evaluation metrics were analyzed, and the significant order of impacts for these influencing factors and their interaction effects was obtained. Through secondary optimization experiments, the optimal parameter combination was determined to be a nozzle-orifice diameter of 1.7 mm, a seed-filling-space angle of 39.3°, and a rotation speed of 657.4 r/min. Static bench-validation tests and indoor vibration-environment simulation experiments were conducted, and the results were compared with a control group. The findings reveal that when the seed-metering plate rotation speed varies between 400 r/min and 1000 r/min, the optimized seed-metering plate exhibits a seed-leakage rate below 7.6% and superior performance in all indicators compared to the original seed-metering plate, indicating a significant improvement in seed-filling efficiency and seed-carrying stability.

Keywords: wheat seed-metering device, pneumatic centrifuge, drag force, DEM-CFD

DOI: 10.25165/j.ijabe.20251805.9438

Citation: Ma D X, Shi S, Li H, Wei G J, Zhou J L, Shi Y P, et al. DEM-CFD-based simulation and optimization of a combined pneumatic-centrifugal wheat seed-metering device. Int J Agric & Biol Eng, 2025; 18(5): 127–141.

1 Introduction

Wheat is a vital staple crop with a long history of cultivation and extensive planting. The practice of three-dimensional uniform seeding in wheat cultivation maintains consistent plant spacing, maximizing the tillering potential of individual wheat plants. The approach offers notable advantages, such as reduced seed usage and enhanced efficiency, making it a pivotal direction for modern mechanized wheat cultivation. For three-dimensional uniform wheat seeding, the seed flow must be measured, uniform, and orderly. To achieve the uniform distribution of seeds, there is an increasing demand for high-quality seeding operations.

High-speed precision-seeding technology plays a fundamental role in enhancing seeding quality and producing quality crops. A seed-metering device is the central component for seeding. Precision wheat seeding generally requires the plants to be spaced within 2-3 cm, which, in turn, mandates the application of higher rotational speeds to the seed-metering device. During high-speed field-seeding operations, the seed-filling efficiency and seed-carrying stability tend to decrease, leading to problems, such as under filling and erroneous cleaning, which subsequently impact the seeding quality. Therefore, enhancing the seed-metering device's operational performance is crucial for improving the seeding quality[1].

Pneumatic seed-metering devices represent one form of wheat-seeding apparatus capable of delivering high precision and operational efficiency. These seed-metering devices can be categorized as central-air conveying collector-type seed-metering devices, suction-type seed-metering devices, and pneumatic-blowing seed-metering devices. In the central-air conveying collector-type seed-metering devices, the seed population is initially blown to the central distribution chamber. It is then further distributed to various end-seeding outlets[2]. Many researchers[3-6] have contributed by analyzing seed trajectories to design critical components that enhance the seed-distribution consistency and supply stability. However, seeds are still dispersed in a disorderly manner, making it challenging to uniformly distribute the wheat in the field and fully harness its tillering potential.

Suction-type and pneumatic-blowing seed-metering devices exhibit reliability issues for seed filling during high-speed operations, often leading to seed leakage. Researchers[7,8] have attempted to address these issues by altering the seed-aggregation state through mechanical stirring, airflow disturbance, and electromagnetic vibration to enhance the seed-filling performance.

Received date: 2024-10-16 **Accepted date:** 2025-05-14

Biographies: Duanxu Ma, MS, research interest: agricultural machinery and equipment, Email: 18805486367@163.com; **Song Shi**, PhD, research interest: agricultural machinery and equipment, Email: shisongfox@163.com; **Hui Li**, PhD, research interest: agricultural machinery and equipment, Email: lihuictrc@shandong.cn; **Guojian Wei**, MS, research interest: agricultural machinery and equipment, Email: woshitxwh@126.com; **Jilei Zhou**, PhD, research interest: agricultural machinery and equipment, Email: zhoujilei@shandong.cn; **Yupeng Shi**, MS, research interest: agricultural machinery and equipment, Email: shiyupeng1997@163.com.

***Corresponding author: Hu Liu**, MS, research interest: agricultural machinery and equipment. Shandong Academy of Agricultural Sciences, Jinan 250100, China. Tel: +86-15305313678, Email: liuhu0725@163.com.

However, these efforts have not fundamentally considered the seed-metering devices' seed-filling method, leaving room for improvement during high-speed operations. This paper presents the design of a combined pneumatic-centrifugal wheat seed-metering device, which employs a combined mechanical–pneumatic seed-filling approach, along with centrifugal seed cleaning, to achieve an ordered and uniform seed arrangement from a centralized pneumatic conveyor-type seeding device.

The seed-filling process in pneumatic seed-metering devices involves complex interactions between the airflow and seeds, making it challenging to quantitatively describe the forces and movement of seeds at different seed-filling stages through traditional methods[9]. With the advancement of computer technology, discrete element method–computational fluid dynamics (DEM-CFD) simulations have been extensively applied to researching the seed-filling process of pneumatic seed-metering devices[10]. The discrete element method (DEM) is an analytical approach based on molecular-dynamics principles, simulating the propagation of movement within a particle group. It calculates the forces acting on various contact points between particles, based on their overlap and tangential displacement in a soft-sphere model. Computational fluid dynamics (CFD) accurately models fluid flow, providing precise insights into the influence of airflow.

To comprehensively describe the interactions between particles and airflow, a DEM-CFD coupling method has been applied to various engineering projects[11,12]. For instance, this method has been utilized in the study of particle-dispersion mechanisms in gas–solid flows[13-18]. In the realm of seed-metering devices, Lei et al.[19] employed the DEM-CFD approach to simulate seed movement in a feeding device, which determined the airflow input velocities. Wang et al.[20] studied seed movement and drag characteristics using the DEM-CFD approach, simulating a "seed–air–soil" coupling model.

In addition, DEM-CFD has been used to conduct numerical studies on airflow and particle movement, simulating the interaction between seeds and airflow in seed-metering devices. This allows for the optimization of mechanical structures to enhance seed-metering device performance[21-28]. Therefore, by combining DEM and CFD and analyzing the results of coupled calculations, it is possible to fully elucidate the mechanics of particle and fluid motion.

The poor seed-filling and carrying performance during high-speed operations, which arises from seed leakage and erroneous seed cleaning, is aimed to be addressed by this study. It proposes a combined mechanical–pneumatic seed-filling approach for the seed-metering device. The approach involves designing the seed-filling-space angle at the nozzle to guide the seed entry and introducing orifice structures at the nozzle to facilitate seed filling with positive-pressure airflow. These modifications enhance the seed-filling efficiency and seed-carrying stability, meeting the demands of precision seeding.

Owing to the relatively small volume of wheat grains, seeds tend to accumulate densely within the seed-metering device. To comprehensively describe the effects of particle–particle and particle–airflow interactions, the DEM-CFD (gas–solid two-phase flow simulation) analysis method is introduced to simulate the seed-metering device's operation process. The seed-filling and seed-cleaning processes were analyzed from both macroscopic and microscopic perspectives in this paper, and the trends in flow field–induced forces on seeds were studied. Based on this analysis, the orifice and seed-filling-space angle parameters were optimized, and the seed-filling performance of the seed-metering device was effectively improved. Experimental data comparisons validate the feasibility and effectiveness of the seed-filling process analysis, based on a DEM-CFD coupling simulation.

2 Overall structure of the seed-metering device and operation procedure

2.1 Structural design of seed-metering device

2.1.1 Overall structure

Figure 1a shows the structure of the combined pneumatic-centrifugal precision wheat seed-metering device. It primarily consists of a front housing, baffles, seed-metering plate, rear housing, base, motor, and other components. The seed-metering device is driven by a servo motor, ensuring precise control of the rotational speed. The entire operation can be divided into four stages: seed filling, seed protection, seed cleaning, and seed discharge.

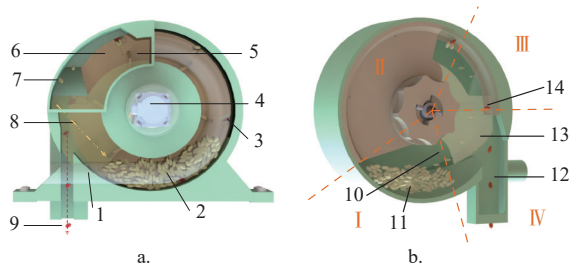

1. Seed-filling pipe; 2. Seed population in the filling zone; 3. Target seeds; 4. Motor; 5. Observation window; 6. Seed-metering plate; 7. Excess seeds removed; 8. Seeds rejoining the filling zone; 9. Seeds discharged in an orderly flow; Ⅰ. Seed-filling stage; Ⅱ. Seed protection stage; Ⅲ. Seed cleaning stage; Ⅳ. Seed discharge stage; 10. Return zone; 11. Seed-filling zone; 12. Seed discharge zone; 13. Baffles; 14. Initial seed drop position.

Figure 1 Overall structure and operating principle of the seed-metering device

As depicted in Figure 1b, under the influence of pneumatic forces, wheat seeds flow through the seed-filling pipe into the chamber, where they descend into the seed-filling area. When the seed-metering plate passes through the seed-filling area, its integrated seed-guide groove structure disrupts and directs the seed population, guiding the seeds along its arc toward the nozzle. An orifice structure is connected to the nozzle.

The orifice chamber has a positive pressure airflow, which exerts pressure on the seeds. Thus, using the combined mechanical structure of the nozzle and the pressure airflow at the orifice, the seed-metering device is filled. The seeds are stably pressed into the nozzle and continue to move along with the seed-metering plate. Baffles divide the internal chamber into a backflow area and a seed-discharge area. During the seed-cleaning stage, excess seeds are cleared away by centrifugal force and return to the seed-filling area through the backflow area. The target seeds that have not been cleared reach the seed-discharge area and are released, resulting in a well-organized and uniform seed flow.

2.1.2 Design of key structural parameters

The seed-metering plate is a crucial component for achieving precise wheat seeding. Its diameter significantly impacts the overall seed-metering device size, number of nozzles, and centrifugal force. During the seed-filling process, the time required for the seed-metering plate to pass through the seed-filling area is directly proportional to the efficiency of the seed-filling operation.

When the forward speed of the unit and the plant spacing are constant, the time required by the seed-metering plate to pass through the seed-filling area is only related to the size of the seed-

filling area and the seed-metering plate's rotational speed. The seed-metering plate's diameter does not directly affect the seed-filling time. However, when the arc length of the seed-metering plate corresponding to the angle of the seed-filling area remains fixed, a larger seed-metering plate diameter accommodates more nozzles. In addition, when the planting spacing is fixed, the number of nozzles affects the rotational speed, thereby influencing the seed-filling time.

In the design of the seed-metering device, the centrifugal seed cleaning is employed, and different rotational speeds yield varying seed-cleaning effects. Therefore, when the seed-filling area has a fixed scope, a larger seed-metering plate diameter would result in a lower rotational speed, reducing the centrifugal force, which is detrimental to clearing excess seeds and could lead to reseeding. Moreover, an increased seed-metering plate diameter would affect the overall structure size and require more material.

Conversely, a smaller seed-metering plate diameter would increase the rotational speed, reducing the individual nozzle's seed-filling time, which is detrimental to the seed-filling efficiency and could cause seed leakage. Furthermore, an excessively high seed-metering plate rotation speed would increase the power consumption. When the planting spacing and structural dimensions are determined, the number of nozzles is negatively correlated with the rotational speed of the seed-metering plate, thus affecting the effect of seed filling and centrifugal force seed cleaning, which is affected by the same mechanism as above. Existing seed-metering plate diameters typically range from 80 to 260 mm. Considering the overall structure, a 160 mm diameter seed-metering plate with six uniformly distributed nozzles was selected.

In the design of the seed-metering device, during seed selection, the seeds are held in a reclined state within the nozzles; the ideal posture after stable clamping is depicted in Figure 2a. The inner side of the nozzle is at an angle α to the horizontal plane of the seed-metering plate, guiding the seeds to smoothly enter the nozzle. Simultaneously, the airflow pressure force can be resolved in the horizontal direction of the seeds. A protruding baffle is placed on one side of the target seeds to support them as they move around the circular path of the seed-metering plate.

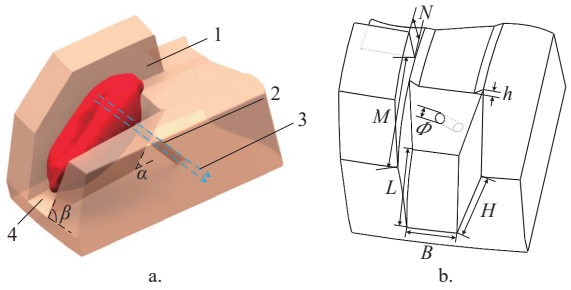

a. b.

1. Upper baffle 2. Nozzle-orifice 3. Positive air pressure 4. Nozzle α. Seed filling angle L. Nozzle length B. Nozzle width H. Nozzle height Φ. Nozzle-orifice diameter h. Seed guide slot depth

Figure 2 Seed-clamping posture and schematic diagram of the nozzle-structure dimensions

To effectively capture individual seeds, the nozzle dimensions should be designed based on the dimensions of wheat seeds. Wheat variety Jimai 22 was selected for testing, and the measured and statistically analyzed average values of the wheat seed's length, width, height, equivalent diameter, and thousand-grain weight were l_a = 6.54 mm, b_a = 3.23 mm, d_a = 3.11 mm, D_z = 3.98 mm, and K = 42.4 g, respectively.

Therefore, based on the ideal clamping state of the seed shape, the dimensions of various structures at the nozzle (as shown in Figure 2b) should satisfy the following equation:

$$\begin{cases} 0.8l_a < L < l_a \\ b_a < B < 1.2b_a \\ 0.8h_a < H < 1.2d_a \end{cases} \tag{1}$$

According to Equation (1), it can be inferred that within the above-mentioned range, the nozzle length L ensures that only one seed can be accommodated in the length direction. The nozzle width is designed in the same manner. The nozzle height H within the above-mentioned range ensures that the seed's center of gravity remains inside the nozzle after entering it. Considering the stirring and jamming effects of the seed-guide groove on the seed, the seed-guide groove depth h should be less than 0.1 D_z. The inner side of the nozzle is equipped with an orifice Φ, ensuring sufficient pressure force while minimizing the area to prevent the seed's edges from sinking into it. Based on actual seed-measurement data, the nozzle length L = 5.5 mm, nozzle width B = 3.5 mm, nozzle height H = 3.2 mm, seed-guide groove height h = 0.2 mm, and nozzle-orifice diameter Φ < 3 mm.

2.2 Seed-movement analysis during precision seeding

2.2.1 Analysis of the seed-filling process

The seed-filling quality is a crucial aspect that ensures the effectiveness of the seed-metering device. In this design, when the seed-metering device is picking up seeds, it does not rely solely on the accumulation of seed populations and their self-gravity for seed filling. Instead, it utilizes the influence of positive-pressure airflow on the target seeds. Different orifice sizes affect the seed-filling efficiency. Hence, to understand the seed movement during seed filling, it is essential to establish a kinematic seed-filling model.

During the seed-filling process, seeds are subjected to the combined effects of airflow, grain, and gravitational fields, resulting in complex force interactions. Within the grain-flow system, each grain experiences forces from the fluid, neighboring grains, and external objects. Therefore, it is feasible to study these two categories of forces separately: motion under fluid effects and motion under the influence of other grains and external objects.

The forces exerted by the flow field on grains include the drag, buoyant, pressure-gradient, Bassetli, Magnus, and Saffman forces, among others[29]. Among these forces, the drag force exerted on seeds in the airflow is the fundamental force governing the interaction between seeds and the fluid. In cases where the relative velocity between fluid and solids is low, other forces can be disregarded, and the primary focus should be on the drag force.

The effects of the traction force on seeds are as follows:

(1) Guiding seeds to move from the seed population towards the nozzle, ultimately filling the nozzle.

(2) Ensuring the stable adhesion of seeds to the nozzle, preventing erroneous cleaning due to centrifugal forces.

The expression for drag force is as follows:

$$F_p = C\frac{1}{2}\rho U^2 A \tag{2}$$

where, F_p is the airflow-pressure adhesion force at the orifice, N; C is the drag coefficient of the object that is flowing; ρ is the fluid density, kg/m^3; U is the airflow velocity, m/s; and A is the cross-sectional area over which the airflow acts on the grains, m^2.

During the seed-filling process, the interactions among seeds primarily hinder their movement. Depending on their moving posture, the seed-filling process can be divided into two stages:

guided seed filling and stable clamping, as illustrated in Figure 3a. As seeds move towards the nozzle, only a few seeds near the nozzle have a chance to enter it, while the other seeds are obstructed by internal frictional forces. In addition, the target seeds with a filling tendency compete to reach the nozzle, which interfere with each other until the dominant target seeds stabilize and adhere to the nozzles, eliminating weaker contenders.

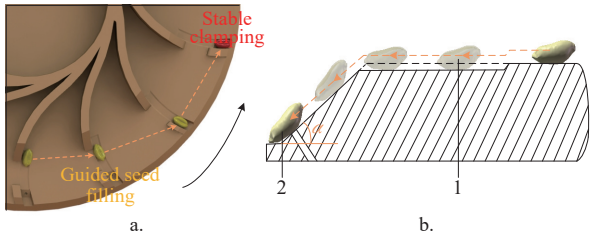

1. Seeds guided by the seed guide slot to slide down; 2. Stabilized clamped target seeds

Figure 3 Schematic diagram of the seed-filling process

Therefore, during the seed's approach to the nozzle, increasing the airflow's effect and thereby enhancing the drag force can effectively increase the chances of seed filling. External forces can also be employed to disrupt the naturally stable accumulation of seed populations, alleviate inter-seed hindrances, and improve the seed-filling probability. Therefore, a combined mechanical-pneumatic seed-filling method was employed in the design of the seed-metering device, which involved a mechanical structure with a seed-guide groove and a nozzle groove of a certain depth.

When the seed-metering plate passes through the seed-filling area, the mechanical structure effectively disrupts the seed population, causing them to "boil" within a certain area, especially dispersing the accumulation of seed populations around the nozzle. This increases the distance between seed particles, reduces the resistance of the seed population during the seed-filling process, and, with the assistance of airflow, effectively enhances the seed filling. On the other hand, by designing the seed-filling-space angle, the force on the target seed can be increased and the difficulty of filling can be reduced, as shown in Figure 3b.

When the target seeds fill into the nozzle, they follow the seed-metering plate in a circular motion. Under the action of gravity, centrifugal force, and the resistance of the surrounding populations, the seeds mainly show a tendency to slide downward out of the nozzle, i.e., a tendency to move in the *x*-axis. After the seed enters the nozzle, the surrounding population still exists to compress the target seed. The forces on the seed in the *z*-axis are mainly downward pressure and drag force, both of which are effective for seed filling. At the same time, under the protection of the nozzle, the target seed movement in the *z*-axis direction is more stable. Therefore, the main movement trend of the target seed is radial movement, and the force in the *x*-axis direction is mainly analyzed, as shown in Figure 4.

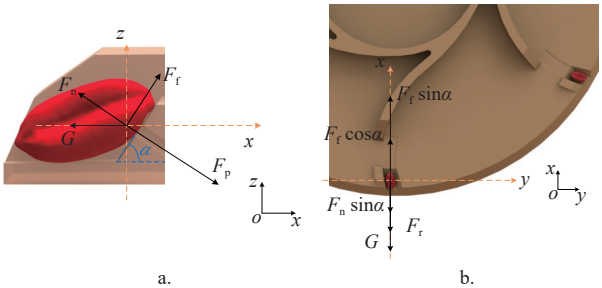

Figure 4 Force analysis

The force analysis for the target seeds is as follows:

$$G + F_r + F_n \sin\alpha = F_p \sin\alpha + F_f \cos\alpha \quad (3)$$

In the equations, G is the gravitational force of the seeds, N; F_r is the centrifugal force acting on the seeds, N; F_n is the support force from the nozzle's inner side in the vertical direction, N; F_p is the airflow-pressure adhesion force at the orifice, N; F_f is the frictional force between the nozzle's inner side and the seeds, N.

From Equations (2) and (3), it can be seen that the tendency of the seeds to move outward can be reduced by increasing the seed-filling-space angle, or by increasing the drag force exerted by the airflow. However, the seed-filling-space cannot be increased indefinitely, which makes it more challenging for seed to enter the nozzle and adversely affects the filling effect. Meanwhile, excessive drag force requires a higher air pressure, leading to excessive power consumption by the machinery, which counters the philosophy of agricultural machinery. Therefore, the orifice size can be adjusted from the perspective of its structure. Under constant air pressure, increasing the orifice area, i.e., increasing the surface area over which the airflow acts on the seeds, generates a greater drag force, while preventing the seeds from jamming with overly large orifices.

2.2.2 Analysis of the seed-carrying process

The seed-carrying performance is a critical factor for ensuring precise seeding. During seed-filling operations, wheat seeds tend to accumulate in huge quantities. After passing through the seed-filling area, the seed-metering plate may carry two or more seeds, which can affect the precise seeding results. Therefore a centrifugal seed-cleaning method is employed in the design.

Once the target seeds enter the nozzle, most of the nozzle space is occupied. As a result, other seeds cannot enter the nozzle and will only move above the target seeds, experiencing an unstable force state. Utilizing the centrifugal force generated by the high-speed rotation of the seed-metering plate, excess seeds are removed in the seed-cleaning area. However, it is essential to preserve the target seeds. Thus, a force analysis of the target seeds is conducted.

When the seed-metering plate reaches the seed-cleaning area, the target seeds tend to move outward, owing to centrifugal forces. These forces are resolved into spatial force components, as shown in Figure 5a (the force on the seed in the nozzle is shown in Figure 4a). During seed-cleaning operations, the nozzle's clamping effect on the seeds primarily prevents seeds from moving outward in the *x*-direction, i.e., radially. Therefore, the forces in the *y*-direction in the spatial force system are not considered for calculation.

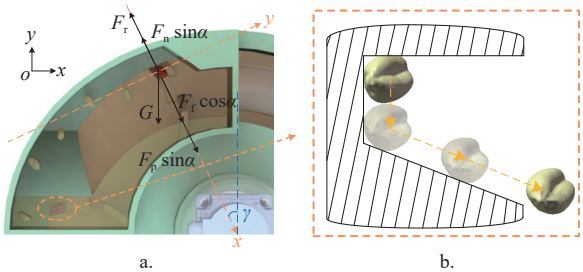

Figure 5 Schematic diagram of the force analysis and discharge process of the target seed

In the *xoy* force system, seeds experience gravitational, centrifugal, pressure-adhesion, and support forces due to pressure adhesion, and frictional force in the *x*-direction. In the *xoz* force system, seeds are subjected to airflow-pressure adhesion force at the orifice, the support force exerted by the nozzle's inner side on the

seeds, and frictional force. At this point, the forces in the *x*-direction can be integrated into the *xoy* force system. The following can be obtained through force analysis:

$$F_x = G\cos\gamma + F_p\sin\alpha + F_f\cos\alpha - F_r - F_n\sin\alpha \quad (4)$$

where, G is the gravitational force of the seeds, N; f is the frictional force between the nozzle's inner side and the seeds, N; F_r is the centrifugal force acting on the seeds, N; F_n is the support force from the nozzle's inner side in the vertical direction, N; γ is the angle formed by the seed-cleaning area and the highest point of the seed-metering plate in degrees, (°).

The seed-cleaning area occurs within 25°-30° after the seed-metering plate reaches its highest point. To ensure that the target seeds in the nozzle are not cleared during seed cleaning, it is necessary to satisfy $F_x > 0$. Therefore, increasing the nozzle-orifice diameter or the seed-filling-space angle can enhance the radial force acting on the seeds, thereby effectively improving the stability of target-seed movement and preventing accidental removal.

Through the above analysis, it is clear that the nozzle-orifice diameter and seed-filling-space angle significantly affect the seed-filling and seed-carrying performance. However, it is unwise to enlarge the nozzle dimensions without restriction due to comprehensive performance considerations. When the seeding implement is engaged in planting operations, as illustrated in Figure 5b, measures are taken to prevent seeds from being subjected to excessive pressure during their movement, which might result in breakage. To this end, a small gap is left between the seeds and the lower surface of the nozzle. As the seeds reach the seed-discharge area, they descend briefly, then slide along the lower surface before being discharged. An excessive nozzle-orifice diameter can lead to seed jamming, negatively affecting the grain-spacing distribution. In addition, an inappropriate seed-metering plate rotation speed can alter the trajectory of the seed descent, reducing the distribution uniformity.

In summary, the analysis of the seed-filling and cleaning processes underscores the significant impact of the nozzle-orifice diameter and the seed-filling-space angle on both the seed-filling performance and seed-carrying stability. Increasing the nozzle-orifice diameter can improve the seed-filling and seed-carrying performance of the seed-metering device, but it is easy to have the phenomenon of seed jamming, which affects the distribution of grain spacing. By changing the angle of the seed-filling space, the pressure adherence of the seed can be increased, but the difficulty of the seed entering the nozzle should also be considered. In addition, the rotation speed will also affect the seed-filling effect and seed uniformity. Therefore, after comprehensive analysis and preliminary tests, the initial range was selected: nozzle-orifice diameter less than 3.0 mm, seed-filling-space angle to be 10°-70°, and rotation speed to be 400-1000 r/min.

However, considering the complexity of seed interactions within the airflow and particle fields, it is difficult to precisely analyze the seed-movement trends. Therefore, a numerical-simulation approach by DEM-CFD was employed to analyze the seed forces during the seed-filling and cleaning processes, further optimizing the critical structural parameters.

3 Simulation materials and methods

3.1 Geometric model

The structural model of the seed-metering device can be simplified into components, such as the housing, seed-metering plate, seed-discharge plate, and nozzle structure, as shown in Figure 6a. This paper selects wheat variety Jimai 22 and utilized a five-axis scanner to obtain a three-dimensional point cloud of the seeds. A solid seed model was created through a reverse engineering process. In the EDEM DEM simulation software, a single grain was replaced with an assembly of multiple sub-grains connected by bonding keys, as shown in Figure 6b. The seeds, upon entering the seed-metering device through the seed-filling pipe, remain in a flowing state and eventually descend to the seed-filling area for the filling operation.

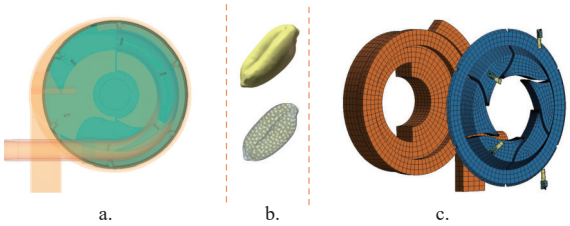

Figure 6 Simplified models of the seed-metering device granular and airflow fields

A three-dimensional airflow-field model for the seed-metering device was constructed using 3D software in this paper, and it was divided into five parts: internal housing chamber, seed-metering plate, seed-guide groove, nozzle, and orifice, as shown in Figure 6c. The grid volume in the flow field was greater than that of the bonded grains. A sliding-mesh technique is employed in this paper, with the regions corresponding to the seed-metering plate, seed-guide groove, nozzle, and orifice designated as moving meshes. The internal housing chamber was kept static. The planes where these parts interface were defined as interfaces for data exchange between the dynamic and static regions. These two parts of the model start simulations in parallel.

3.2 Computational conditions and parameter settings

The wheat-planting spacing was set to 0.03 m. When the seed-metering device operated at a speed of 5 km/h, the seed-metering plate rotated at 74 rad/s. The air pressure at the seed-filling pipe inlet was 5 kPa. The seed-particle generation rate was set at 100 per second. In the initial simulation stages, it was observed that a certain amount of time was required for the particles to be transported to the seed-filling area after generation. Based on multiple simulation experiments, it was determined that the seed-metering plate began to capture seeds after 0.4 s of simulation. The particle interactions followed the standard Hertz–Mindlin (no slip) model. The simulation time step for the particles was set to 2×10^{-6} s, while it was set to 2×10^{-5} s for the airflow field. The parameters for the wheat particles and seed-metering device materials are listed in Table 1.

Table 1 Simulation parameter settings

Parameters	Wheat particles	Resin
Poisson's ratio	0.42	0.39
Shear modulus /Pa	5×10^{8}	3.19×10^{8}
Density /(g·cm^{-3})	1.35	1.02
Coefficient of restitution (with particles)	0.42	0.51
Static-friction coefficient (with particles)	0.53	0.55
Rolling-friction coefficient (with particles)	0.075	0.05

During the seed-metering device operation, the seeds interact with each other, in addition to the airflow, constituting a granular flow field system. Given the small volume of wheat seeds, they are densely packed within the seed-metering device chamber. Therefore, during the simulation analysis, it is crucial to consider

the impact of particles on the airflow field.

To account for this, this paper employs a Eulerian two-way coupling model. The seed-filling pipe was set as an airflow-inlet boundary condition, and the seed-discharge pipe outlet was set as a pressure-outlet boundary condition. The standard k-ε turbulence model was used. The dynamic-mesh region matched the seed-metering plate rotation speed in EDEM, which was 74 rad/s. To obtain detailed information about the seed behavior within the flow field, data were saved every 500 steps, with a time step of 1×10^{-4} s. The total simulation steps were set to 20 000, and a transient calculation method was employed.

3.3 Experimental design

3.3.1 Single-factor experimental design

Based on the simulation results, the seed-metering device's seed-filling and seed-carrying processes were analyzed from both macroscopic and microscopic perspectives. Single-factor experiments were carried out, considering the nozzle-orifice diameter, seed-filling-space angle, and seed-metering plate rotation speed as influencing factors. At the microscopic level, the nozzle void fraction, resistance to clearing, and initial dropping position were selected as performance-evaluation indicators for seed filling and seed carrying. The goal was to determine the ranges of these influencing factors for improved performance. The single-factor experimental factor codes are listed in Table 2.

Table 2 Single-factor experimental factor codes

Number	Factor		
	Nozzle-orifice diameter/mm	Seed-filling-space angle/(°)	Rotation speed/r·min^{-1}
1	0	10	400
2	0.5	20	500
3	1	30	600
4	1.5	40	700
5	2	50	800
6	2.5	60	900
7	3	70	1000

3.3.2 Orthogonal experimental design

Building upon the results of the single-factor experiments, a second-order orthogonal-rotating combination experiment was conducted to determine the optimal parameter combinations for nozzle-orifice diameter, seed-filling-space angle, and rotation speed. The orthogonal experimental codes are listed in Table 3. The total simulation duration was set to 3 s, with the analysis focusing on seed occurrences from 150 consecutive nozzles from a macroscopic perspective. The evaluation metric included the seed-leakage rate, reseeding rate, and grain-spacing qualification rate. The corresponding formulas are as follows:

$$\begin{cases} L_1 = \dfrac{l_1}{l}\times100\% \\ L_2 = \dfrac{l_2}{y}\times100\% \\ L_3 = \dfrac{l_3}{l-l_1-l_2}\times100\% \end{cases} \tag{5}$$

where, L_1 is the seed-leakage rate, %; L_2 is the reseeding rate, %; L_3 is the grain-spacing qualification rate, %; l is the theoretical total number of seeds to be sown; l_1 is the number of nozzles with zero seeds during sowing; l_2 is the number of nozzles with two or more seeds during sowing; and l_3 is the number of individual seeds that descend smoothly.

Table 3 Orthogonal experimental factor codes

Number	Factor		
	Nozzle-orifice diameter/mm	Seed-filling-space angle/(°)	Rotation speed/r·min^{-1}
−1.682	0.8	20	450
−1	1.1	28	531
0	1.6	40	650
1	2.1	52	769
1.682	2.4	60	850

4 Results and discussion

4.1 Analysis of the simulation and modeling process

Figure 7 shows the gas–solid coupled simulation results for the wheat seed-metering device operating at a rotational speed of 74 r/s, with 1.2 mm diameter orifices, and a corresponding angular position of 45° in the seed-filling-space.

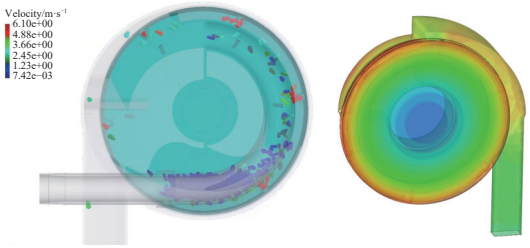

a. Particle fields b. Airflow fields

Figure 7 Simulation results

The trajectories of the airflow in the flow fields are shown in Figure 8a. The trajectories of the particles in the particle fields are shown in Figure 8b. It can be seen that the airflow produces a vertical downward adsorption effect at the nozzles, and the magnitude of the force is affected by the diameter of the nozzle-orifice. When passing through the seed population, the airflow effect at the nozzle-orifice can assist in guiding the seeds into the type nozzle. When the target seed successfully enters the nozzle, there is a pressure difference between the top and bottom of the seed, so it can provide a certain pressure adsorption force for the target seed, which improves the seed-filling effect and the stability of seed transportation. The simulation results verify again the theoretical analysis that increasing the diameter of the nozzle-orifice can improve the seed-filling and seed-carrying performance of the seed discharge.

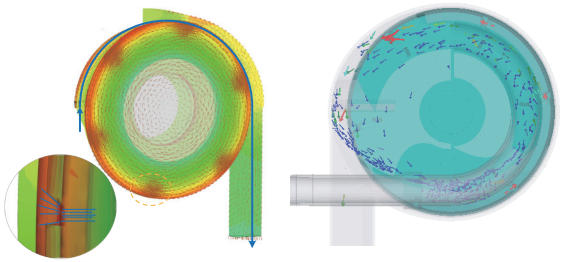

a. Airflow trajectories b. Particle trajectories

Figure 8 Trajectories trend

To assess the variation in the number of seeds within the nozzle, the nozzle void fraction[30] is used as an evaluation metric. An observation area (geometry bin) is defined at each nozzle, extending from the nozzle to the highest point of the baffle, allowing for the calculation of the total particle volume within the observation area at each moment, as shown in Figure 9. The formula for calculating the nozzle void fraction is as follows:

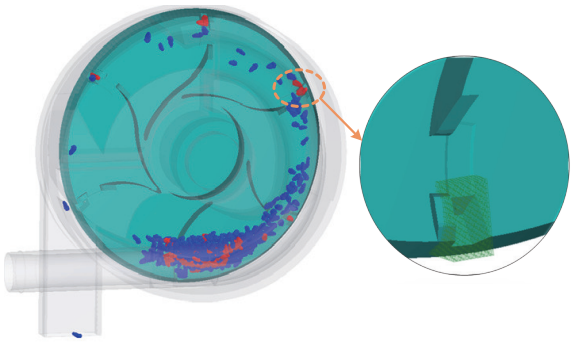

Figure 9 Observation area

$$T = \left(1 - \frac{V_k}{V_g}\right) \times 100\% \tag{6}$$

where, T is the nozzle void fraction, %; V_k is the volume occupied by seed particles, m^3; and V_g is the total volume of the observation area, m^3.

Under the current simulation conditions, the nozzle void-fraction variation curve is extracted from the observation area of a single nozzle throughout the entire operational process, as shown in Figure 10a. Based on the pattern of the curve, the operational process can be divided into four stages:

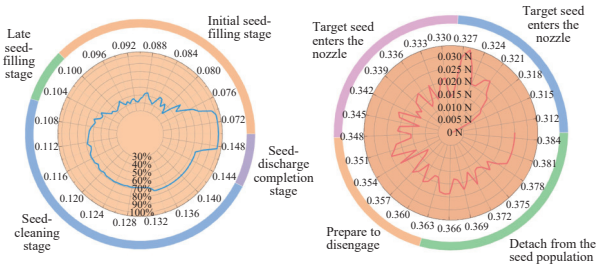

a. Nozzle void fraction b. Coupling-force

Figure 10 Variation curve

Stage Ⅰ. Seed-discharge completion stage: At this point, the nozzle has just completed the seeding operation within the seed-discharge area. The nozzle void fraction rapidly increases from a stable value. During this stage, the nozzle has not yet entered the seed-filling area and is unaffected by seeds, resulting in a final nozzle void fraction of 100%.

Stage Ⅱ. Initial seed-filling stage: As the seed-metering plate rotates, the nozzle gradually enters the seed-filling area. Seeds start to flow towards the nozzle, gradually occupying the observation area within the nozzle. This leads to a sharp decrease in the nozzle void fraction.

Stage Ⅲ. Late seed-filling stage: When seeds occupy the nozzle space, they begin to experience complex forces from the surrounding seed population, including rotation, motion, and potential replacement by other seeds within the population. During this stage, the nozzle void fraction experiences relatively small fluctuations. As the seed approaches detachment from the population, the influence of the surrounding population diminishes, causing the nozzle void fraction to gradually increase.

Stage Ⅳ. Seed-cleaning stage: After the nozzle exits the seed-filling area and enters the seed-cleaning area, any excess seeds it carries are gradually removed. Only the target seeds remain within the nozzle. During this stage, the nozzle void fraction gradually increases until it stabilizes at a certain value.

After passing through the seed-discharge area, the process reverts to the seed-discharge completion stage (Stage Ⅰ), where the nozzle void fraction returns to a stable value of 100%, and the cycle repeats.

In Stage Ⅲ, during the late seed-filling stage, smaller variations in the nozzle void fraction indicate that target seeds experience more stable forces and are less prone to being cleared. This phase represents reliable seed filling within the nozzle. Therefore, the nozzle void-fraction change in the late seed-filling stage (Stage Ⅲ) is adopted as an evaluation metric to analyze its trend under different nozzle-orifice diameters and seed-filling-space angles.

In the context of coupled simulation and modeling, the coupling interface between EDEM and the Fluent fluid-simulation software primarily calculates drag and buoyancy forces. Data storage and retrieval are facilitated through custom attribute functions within the API. The calculation formulas are defined as follows:

$$F_o = m\frac{\mathrm{d}v}{\mathrm{d}t} - G - F_z \tag{7}$$

where, F_o is the coupling force acting on the target seed, N; m is the mass of the target seed, kg; dv/dt is the acceleration of the target seed, m/s^2; G is the gravitational force acting on the target seed, N; and F_z is the contact force between the geometric body and other seeds acting on the target seed, N.

The change in coupling force for target seeds successfully entering the nozzle is depicted in Figure 10b. When the nozzle has not yet entered the seed-filling area, the variation in coupling force is not significant. Starting from 0.075 s after entering the seed-filling area, the coupling force on the seeds rapidly increases, followed by repeated declines. This phenomenon is attributed to the attraction of seeds by the nozzle, resulting in seed migration. At 0.09 s, when the target seed enters the nozzle, the coupling force begins to fluctuate within a certain range. During this phase, the seed is compressed and collides with the surrounding seed population, leading to an unstable state.

At 0.103 s, as the seed is about to detach from the population, the resistance from surrounding seeds intensifies, causing greater fluctuations in the coupling force. At 0.112 s, upon detachment from the population, the number of surrounding seeds decreases. The coupling force on the seed increases to a certain extent. Ultimately, only the target seed and a few excess seeds from the surroundings are carried away, resulting in slight fluctuations in the coupling force within a certain range. In this phase, the coupling force continues to fluctuate but with a lower frequency and intensity than the previous phase.

Once the seed enters the seed-cleaning area, excess seeds are removed by centrifugal forces, causing the coupling force on the target seed to increase until it stabilizes. At this point, only the target seeds remain within the nozzle, and the seed remains stable, as shown in Figure 11. The stable coupling force achieved during this phase represents the main force resisting seed removal, i.e., the resistance to clearing. The stable coupling force is selected as the evaluation metric for seed-carrying stability.

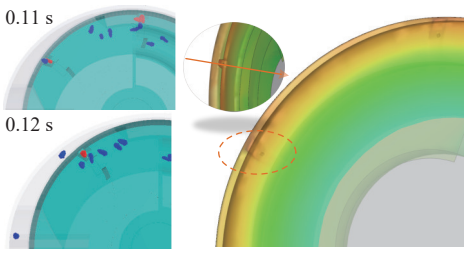

Figure 11 Coupling-force variation diagram

As the seed-metering plate traverses the seed-discharge area, seeds should slide out of the nozzle within a specified time frame. Based on multiple simulation tests, it was observed that if the seed's initial dropping position falls within seed-discharge area *b* in Figure 12, the seed-descent process will not contact the sidewalls, allowing for a smooth descent. If the seed falls within seed-discharge area *a*, it will contact the left sidewall during descent. Seeds falling within seed-discharge area *c* will contact the right sidewall during descent. Both sidewall-contact scenarios alter the seed's trajectory, resulting in uneven grain spacing.

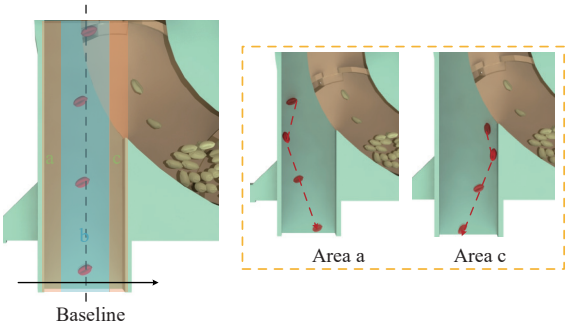

Figure 12 Schematic diagram of the seed-discharge process

Consequently, in simulation experiments, data regarding the initial seed-dropping position, with the arrow denoting the positive direction, were collected to determine the horizontal coordinates of the initial dropping position. These coordinates serve as the evaluation metric for analyzing the grain-spacing distribution effect under different nozzle-orifice diameters and rotational speeds.

4.2 Analysis of single-factor experimental results

4.2.1 Analysis of the influence of the nozzle-orifice diameter on performance metrics

The nozzle-orifice diameter affects the seed-nozzle void fraction, resistance to clearing, and initial dropping position, as shown in Figure 13. As the nozzle-orifice diameter increases, the change in nozzle void fraction gradually decreases, and the resistance-to-clearing value increases. For example, when the nozzle-orifice diameter increases from 0.5 to 1.5 mm, the nozzle void-fraction change decreases from 34% to 18%, and the resistance to clearing increases from 0.0066 to 0.016 N. This indicates that the seed-filling performance and seed-carrying stability improve with an increase in nozzle-orifice diameter.

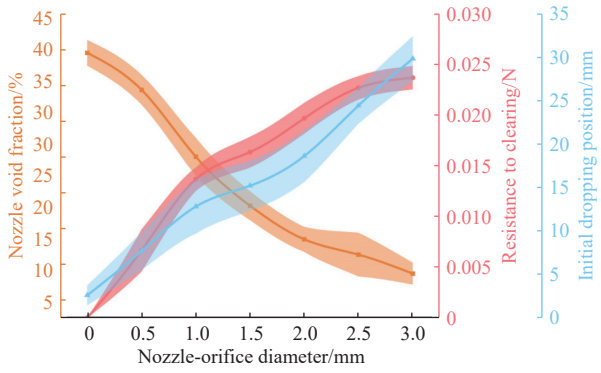

Figure 13 Trends in orifice-diameter effects

A larger nozzle-orifice diameter results in an increased drag force on seeds during the filling operation, reducing the interference of other seeds. It also helps resist the outward radial movement of seeds during the clearing operation, ensuring reliable seed filling and carrying.

However, with an increase in nozzle-orifice diameter, the horizontal coordinate of the seed's initial dropping position gradually enters the unacceptable zone. This is because an excessively large nozzle-orifice diameter can cause some seed volume to become stuck in the nozzle, and the seed is subjected to an excessive drag force. All these factors prevent seeds from dropping within the specified time, affecting the grain-spacing distribution. Therefore, it is essential to limit the nozzle-orifice diameter.

4.2.2 Analysis of the influence of the seed-filling-space angle on performance metrics

The seed-filling-space angle affects the seed-nozzle void fraction and resistance to clearing, as shown in Figure 14. As the seed-filling-space angle increases, the change in nozzle void fraction decreases, and the resistance-to-clearing value increases. For example, as the seed-filling-space angle increases from 20° to 40°, the nozzle void-fraction change decreases from 26% to 20%, and the resistance to clearing increases from 0.002 N to 0.011 N. This indicates that the seed-filling performance and seed-carrying stability improve with an increase in the seed-filling-space angle. As the seed-filling-space angle becomes larger, the seeds are subjected to a greater radial inward component of the drag force acting on them. This helps resist their outward radial movement.

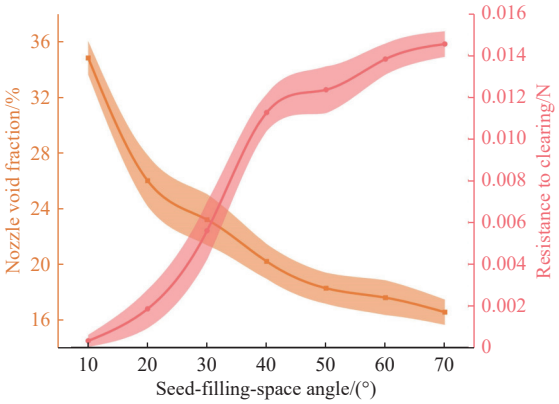

Figure 14 Trends in seed-filling-space angle effects

It can be observed that changing the seed-filling-space angle and increasing the nozzle-orifice diameter have similar effects on the filling performance and seed-carrying stability. However, within the same change trend, the impact of the seed-filling-space angle on the nozzle void-fraction change is smaller than that of the nozzle-orifice diameter. In addition, the numerical values of resistance to clearing corresponding to the seed-filling-space angle are also smaller than those corresponding to the nozzle-orifice diameter. It can be shown that the influence of the nozzle-orifice diameter on the seed-filling and seed-carrying performance is greater than that of the seed-filling-space angle. This is because the improvement of the seed-filling performance and seed-carrying stability essentially increases the magnitude of the drag force on the seeds. Therefore, altering the nozzle-orifice diameter is the most direct approach to achieve this goal.

4.2.3 Analysis of the influence of the rotation speed on performance metrics

The rotation speed affects the seed-nozzle void fraction and initial dropping position, as shown in Figure 15. With increasing rotation speed, the change in the nozzle void fraction increases, and the initial dropping position tends toward the unacceptable zone. For example, as the rotation speed increases from 500 to 700 r/min, the nozzle void-fraction change increases from 21% to 29%, indicating a decrease in the seed-filling and seeding performance. This is because, at high speeds, the seed-metering plate passes through the filling area more quickly, reducing the filling time.

Moreover, when seeds enter the orifice, they collide with other seeds, resulting in a more pronounced change in the nozzle void fraction. Therefore, as the seeds drop, they have not had sufficient time to drop within the ideal area, owing to the shorter time, leading to poor grain-spacing uniformity.

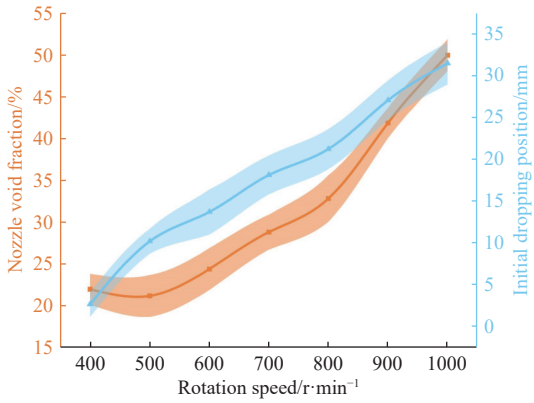

Figure 15 Trends in rotation speed effects

4.2.4 Discussion of experimental results

Based on analysis of single-factor experimental results, the parameters can be further optimized as follows: the nozzle-orifice diameter to be 0.8-2.4 mm, the seed-filling-space angle to be 20°-60°, and the rotation speed to be 450-850 r/min.

The seed-filling performance and seed-carrying stability have a crucial impact on the quality of the seed-metering device's operation. Therefore, it is essential to explore various influencing factors under the optimal working performance. The analysis of single-factor experimental results suggests that performance metrics related to seed filling and seed carrying might be influenced by multiple factors, and one factor might affect multiple indicators. For instance, the nozzle void fraction is influenced by the nozzle-orifice diameter, seed-filling-space angle, and rotation speed. The nozzle-orifice diameter affects the nozzle void fraction, resistance to clearing, and initial dropping position.

Observing the seed-metering device performance at a microscopic scale has certain limitations. For example, the nozzle-orifice diameter has a positive and negative feedback effect on the seed-filling and seed-carrying performance. Increasing the nozzle-orifice diameter improves the seed-metering device performance; however, an excessively large nozzle-orifice diameter affects the grain-spacing distribution. Therefore, at a macroscopic scale, parameters such as the seed-leakage rate, reseeding rate, and grain-spacing qualification rate are defined as performance metrics for seed filling and carrying.

The reasonable ranges of each factor obtained from single-factor experimental results are used as values, considering the interaction between various influencing factors. Therefore, quadratic orthogonal-rotation combination experiments are conducted to seek the optimal working parameters.

4.3 Parameter optimization

4.3.1 Analysis of orthogonal experimental results

The orthogonal experimental factors and indicators are presented in Table 4. The results of the variance analysis are listed in Table 5.

Table 4 Experimental factors and indicators

No.	Nozzle-orifice diameter/mm	Seed-filling-space angle/(°)	Rotation speed/ r·min⁻¹	Seed-leakage rate/%	Reseeding rate/%	Grain-spacing qualification rate/%
1	–1	–1	–1	8.87	7.1	84.03
2	1	–1	–1	5.66	8.42	85.92
3	–1	1	–1	9.89	8.98	81.13
4	1	1	–1	4.48	9.21	86.31
5	–1	–1	1	9.98	1.69	88.33
6	1	–1	1	9.76	4.59	85.65
7	–1	1	1	8.48	7.86	83.66
8	1	1	1	4.67	8.31	87.02
9	–1.682	0	0	9.92	3.74	86.34
10	1.682	0	0	5.31	5.41	89.28
11	0	–1.682	0	9.13	4.27	86.6
12	0	1.682	0	5.87	8.96	85.17
13	0	0	–1.682	5.07	10.53	84.4
14	0	0	1.682	8.32	6.77	84.91
15	0	0	0	3.6	3.62	92.78
16	0	0	0	3.34	3.55	93.11
17	0	0	0	4.42	3.3	92.28
18	0	0	0	3.75	3.19	93.06
19	0	0	0	2.96	3.08	93.96
20	0	0	0	3.16	3.01	93.83
21	0	0	0	3.02	3.69	93.29
22	0	0	0	2.61	3.12	94.27
23	0	0	0	3.42	3.54	93.04

Table 5 Variance analysis

Variance source	Seed-leakage rate			Reseeding rate			Grain-spacing qualification rate		
	Sum of squares	F	p	Sum of squares	F	p	Sum of squares	F	p
Model	156.56	64.06	< 0.0001**	150.28	163.38	< 0.0001**	371.67	78.01	< 0.0001**
x_1	30.48	112.24	< 0.0001**	4.35	42.57	< 0.0001**	11.80	22.29	0.0004**
x_2	10.96	40.35	< 0.0001**	30.62	299.55	< 0.0001**	4.94	9.33	0.0092**
x_3	6.55	24.11	0.0003**	22.64	221.52	< 0.0001**	4.84	9.14	0.0098**
x_1x_2	4.19	15.43	0.0017**	1.57	15.33	0.0018**	10.88	20.56	0.0006**
x_1x_3	2.63	9.70	0.0082**	0.4050	3.96	0.0680	5.10	9.64	0.0084**
x_2x_3	5.17	19.03	0.0008**	6.52	63.76	< 0.0001**	0.0780	0.1474	0.7073
x_1^2	38.06	140.16	< 0.0001**	3.63	35.56	< 0.0001**	65.22	123.21	< 0.0001**
x_2^2	36.09	132.90	< 0.0001**	22.86	223.70	< 0.0001**	116.40	219.89	< 0.0001**
x_3^2	23.75	87.44	< 0.0001**	58.51	572.53	< 0.0001**	156.81	296.23	< 0.0001**
Residual	3.53			1.33			6.88		
Lack of fit	1.32	0.9499	0.4992	0.7948	2.38	0.1319	3.75	1.92	0.1967
Pure error	2.22			0.5338			3.13		
Cor total	160.09			151.61			378.55		

Note: ** highly significant (p<0.01); * significant (0.01<p<0.05).

Based on the variance-analysis results in Table 5, the factors affecting the seed-leakage rate can be ranked in descending order of impact as nozzle-orifice diameter, seed-filling-space angle, and rotation speed. Among them, the effects of the nozzle-orifice diameter, seed-filling-space angle, and rotation speed on the seed-leakage rate are highly significant. Meanwhile, the interaction of nozzle-orifice diameter and seed-filling-space angle, nozzle-orifice diameter and rotation speed, as well as seed-filling-space angle and rotation speed had highly significant effects on the seed-leakage rate.

The factors affecting the reseeding rate can be ranked in descending order of impact as seed-filling-space angle, rotation speed, and nozzle-orifice diameter. Among them, the effects of the seed-filling-space angle, rotation speed, and nozzle-orifice diameter are highly significant. Meanwhile, the interactions between the seed-filling-space angle and rotation speed, as well as between the nozzle-orifice diameter and rotation speed, significantly affect the reseeding rate.

The factors affecting the grain-spacing qualification rate can be ranked in descending order of impact as nozzle-orifice diameter, seed-filling-space angle, and rotation speed. Among them, the effects of the nozzle-orifice diameter, seed-filling-space angle, and rotation speed on the grain-spacing qualification rate are highly significant. Meanwhile, the interactions between the nozzle-orifice diameter and seed-filling-space angle, as well as between the nozzle-orifice diameter and rotation speed, significantly affect the grain-spacing qualification rate.

After excluding non-significant factors, the regression equations for each indicator are as follows:

$$L_1 = 3.36 - 1.49X_1 - 0.9X_2 + 0.69X_3 - 0.72X_1X_2 + 0.57X_1X_3 - 0.8X_2X_3 + 1.55X_1^2 + 1.51X_2^2 + 1.22X_3^2 \quad (8)$$

$$L_2 = 3.34 + 0.56X_1 + 1.5X_2 - 1.29X_3 - 0.44X_1X_2 + 0.9X_2X_3 + 0.48X_1^2 + 1.2X_2^2 + 1.92X_3^2 \quad (9)$$

$$L_3 = 93.3 + 0.93X_1 - 0.6X_2 + 0.6X_3 + 1.17X_1X_2 - 0.8X_1X_3 - 2.03X_1^2 - 2.71X_2^2 - 3.14X_3^2 \quad (10)$$

After eliminating non-significant factors, the determination coefficients (R^2) for each indicator's regression equations are 0.96, 0.98, and 0.97, indicating the significance of the established regression models. The predicted values from the regression equations are accurate in relation to the actual values. To visually demonstrate the influence of interaction effects between factors on the seed-metering device performance, response-surface plots for the nozzle-orifice diameter, seed-filling-space angle, and rotation speed on the seed-leakage rate, reseeding rate, and grain-spacing qualification rate were generated using the Design-Expert experimental-design software, as shown in Figure 16.

From Figures 16a, 16d, and 16g, it can be observed that increasing the nozzle-orifice diameter enhances the seed adhesion and reduces the seed-leakage rate. Similarly, it can be deduced that

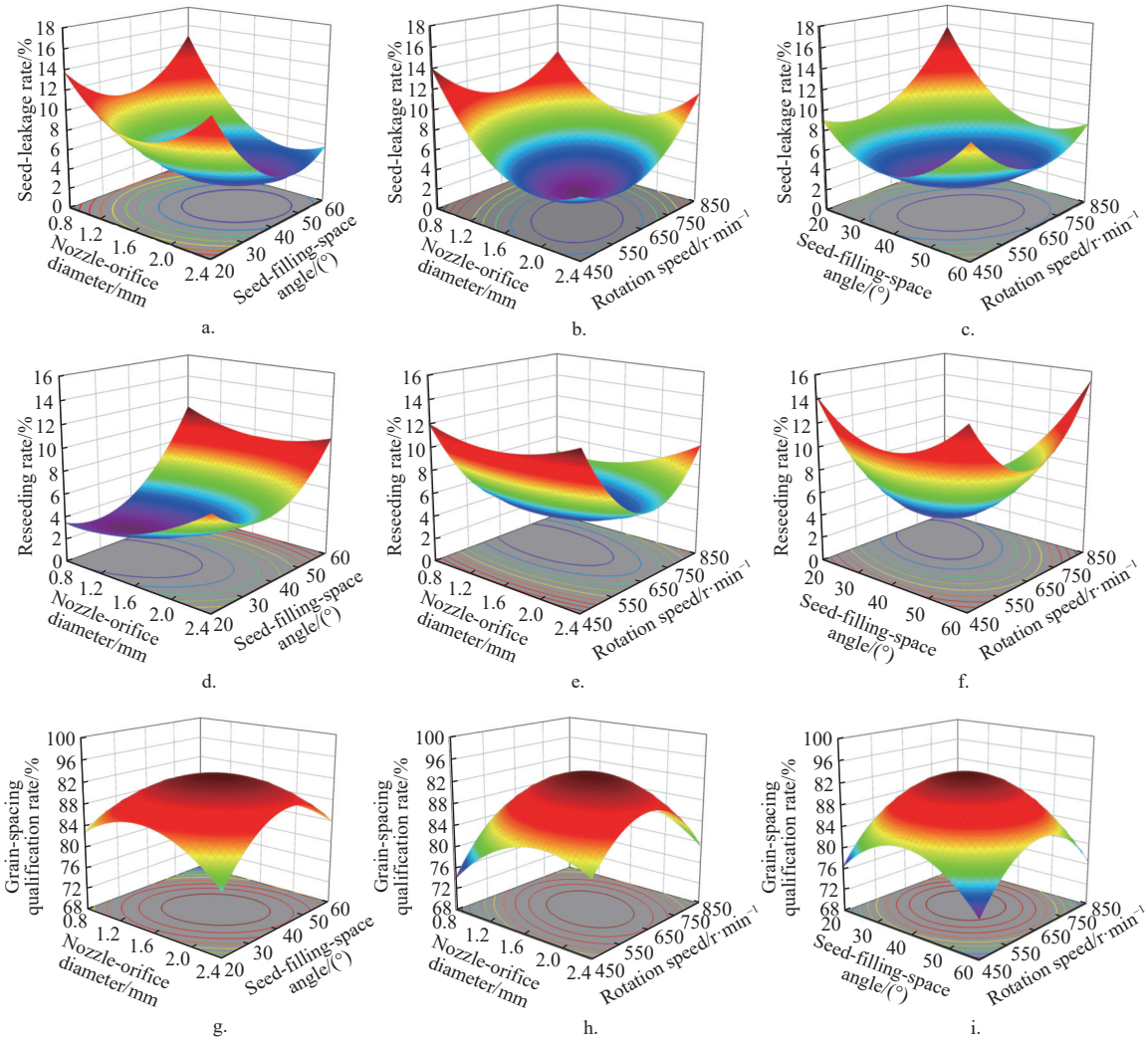

Figure 16 Response-surface and contour plots of the experimental factors on the indicators

enlarging the seed-filling-space angle reduces the difficulty of successful adhesion of target seeds, leading to a decrease in the seed-leakage rate. However, the reseeding rate increases, and the grain-spacing qualification rate decreases. From Figures 16b, 16e, and 16h, it is evident that a high rotation speed generates a greater centrifugal force, reducing the reseeding rate but adversely affecting the seed-filling performance, leading to a higher seed-leakage rate.

4.3.2 Optimization

The optimization module of the Design-Expert software is used to obtain the optimal combination of factors for the seed-metering device's best performance. The goal is to minimize the seed-leakage rate and reseeding rate, while maximizing the grain-spacing qualification rate. The regression model is solved by multi-objective optimization with the following optimization objective function and constraints:

$$\begin{cases} \min Y_1(x_1, x_2, x_3) \\ \min Y_2(x_1, x_2, x_3) \\ \max Y_3(x_1, x_2, x_3) \\ \text{s.t.} \begin{cases} 0.8\ \text{mm} \le x_1 \le 2.4\ \text{mm} \\ 20^\circ \le x_2 \le 60^\circ \\ 450\ \text{r/min} \le x_3 \le 850\ \text{r/min} \end{cases} \end{cases} \tag{11}$$

By substituting the data and solving, the optimal operating parameters were found to be as follows: The nozzle-orifice diameter is 1.7 mm, the seed-filling-space angle is 39.3°, and the rotation speed is 657.4 r/min. At these settings, the seed-metering device's seed-leakage rate is 3.24%, reseeding rate is 3.33%, and grain-spacing qualification rate is 93.43%.

4.3.3 Validation of optimization results

In order to verify the accuracy of the simulation optimization, the coupling simulation is performed again based on the optimization results. The simulation parameters are set as follows: the nozzle-orifice diameter is 1.7 mm, the seed-filling-space angle is 39.3°, and the rotation speed is 657.4 r/min. Multiple experiments are carried out on the premise that other factors are not changed. The results show that the average values of each evaluation metric are as follows: the seed-leakage rate of the seed-metering device is 3.36%, reseeding rate is 3.51%, and grain-spacing qualification rate is 93.13%. The experimental results are basically consistent with the optimization results.

4.4 Model validation

4.4.1 Static bench validation

To validate the simulation results of the designed seed-metering device, static bench comparative tests were conducted using four different combinations of seed-metering plate structures with varying parameters. Optimized seed-metering plate *A* was used as the test group, with an inner-side nozzle-orifice diameter of 1.7 mm and a seed-filling-space angle of 39.3°. The structural parameters of seed-metering plate *B* before optimization were set at their limit levels. Seed-metering plates *C* and *D* had restrictions on the nozzle-orifice diameter and seed-filling-space angle, respectively. The specific parameters of different combinations are listed in Table 6.

The designed seed-metering plate main body and nozzle were detachable and 3D printed for ease of structure replacement. The test setup was as shown in Figure 17. The seed-metering device was attached to the end of the seed-delivery pipe and independently driven by an ECMA-C10401ES servo motor. This motor had a torque of 0.3 N·m, and its speed could be precisely controlled within 3000 r/min, meeting the requirements for high-speed testing.

Table 6 Structural parameters of the seed-metering plates in the validation test

Parameters	Test group	Control group		
	A	*B*	*C*	*D*
Number of nozzles	6	6	6	6
Nozzle-orifice diameter/mm	1.7	0	0	1.7
Seed-filling-space angle/(°)	39.3	70	39.3	70

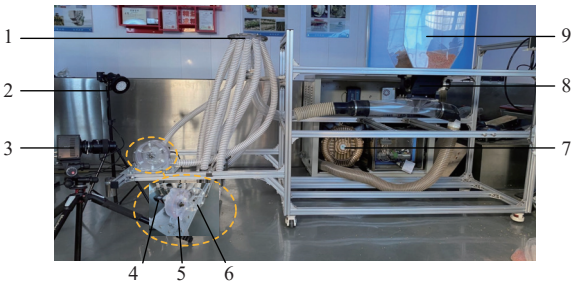

1. Distributor 2. Lightening device 3. High-speed camera 4. Servo motor 5. Seed-metering device housings 6. Seed-metering plate 7. Seed-delivery pipe 8. Fan 9. Central conveying device

Figure 17 Static bench test setup for seed-metering device

A high-speed camera was used to record the seed-metering device's operation. In the test, the movement of seeds in the observation and seed-dropping areas was recorded using high-speed photography. The seed-metering plate rotation speeds were set at seven levels: 400, 500, 600, 700, 800, 900, and 1000 r/min. The seed-leakage rate and reseeding rate were the main indicators, with each group of seeds counted up to 1000, and each test repeated five times.

The test results, shown in Figure 18, present the mean values and standard deviations for various test indicators. From the test results, it can be observed that although the reseeding rate of seed-metering plate *B* before optimization is low, its seed-leakage rate is significantly higher than those of the other groups. Moreover, as the speed increases, the seed-leakage rate exhibits a larger variation range, indicating an obvious decrease in seed-filling performance.

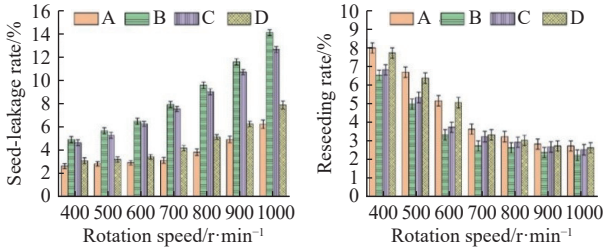

Figure 18 Static bench test results

Comparing the working effects of seed-metering plates *A* and *B* before and after optimization, it is obvious that the seed-leakage rate of seed-metering plate *B* is significantly higher than that of *A* at higher speeds. Seed-metering plate *C* has a lower reseeding rate than *A* and *D*, and its seed-leakage rate does not change significantly at lower speeds. However, when the speed exceeds 600 r/min, the seed-leakage rate shows a rapid increase. Seed-metering plates *A* and *D* have similar variations in the reseeding rate and seed-leakage rate, with small changes in the seed-leakage rate and a gradual convergence of reseeding-rate values with increasing speed.

At a speed of 600 r/min, the seed-leakage rate for plate *A* is 2.89%, while for plate *D* it is 3.4%. When the speed is increased to

700 r/min, the seed-leakage rate for plate *A* is 3.09%, and for plate *D* it is 4.15%. Therefore, at different speed levels, the seed-leakage rate for plate *A* is consistently lower than that for plate *D*. It can be concluded that plate *A* has a more pronounced effect in countering adverse factors affecting seed filling and better meets the seed-filling requirements for high-speed operations.

4.4.2 Simulation validation in a vibrating environment

During field-seeding operations, the seed-metering device does not operate under stable conditions, owing to factors such as uneven terrain and the seed-metering device's own vibrations. However, for seed-metering device installation requirements and the feasibility of using high-speed camera equipment, it is impossible to directly observe the internal seed movement of the seed-metering device during field operations. As a result, it is challenging to conduct an intuitive analysis of the seed-metering device's performance during various stages of operation. To better align with practical production, the designed seed-metering device was placed on a vibration test bench for simulation testing. This allowed for an assessment of the seed-metering device's performance in a field working environment.

On October 20, 2022, during wheat-seeding operations in Qihe County, Dezhou City, China, vibration data-acquisition sensors were scattered and installed at multiple positions on the seed-metering device to collect random vibration signals during operation. The Siemens vibration and noise-acquisition analysis system (LMS, Leuven Measurement Systems) was used, and the sensors were integrated-circuit piezoelectric (ICP) triaxial accelerometers from PCB Piezotronics, Inc.

The seeding was performed using a 2BQJM-24 pneumatic ground wheat-seeding combine harvester. The harvester had two large-capacity groove wheel-type seed-metering devices connected to the bottom of the seed box, supplying seeds to the distributor. The distributor uniformly distributed the incoming seed flow to the end units, with each distributor corresponding to 12 units, enabling seeding in 24 rows in a single operation. Six different positions on the harvester were selected as measurement points, and sensors were placed to collect vibration signals during field operations, as shown in Figure 19.

Figure 19 Vibration-signal collection during harvester field operation

To minimize the influence of random errors, three measurement points were selected on the end of the seed-metering device: the second unit on the left, the second unit on the right, and the central unit. These points served as data sources for the field-vibration signals of the designed seed-metering device. Random vibration signals were collected in the longitudinal, transverse, and vertical directions of the seed-metering device, at seven different speed levels corresponding to the seed-metering device's rotational speeds: 400, 500, 600, 700, 800, 900, and 1000 r/min. Each data collection lasted for a minimum of 30 s, and each group was repeated three times. Figure 20a depicts the acceleration signals in three-dimensional directions for the selected central unit when the rotational speed was set at 700 r/min.

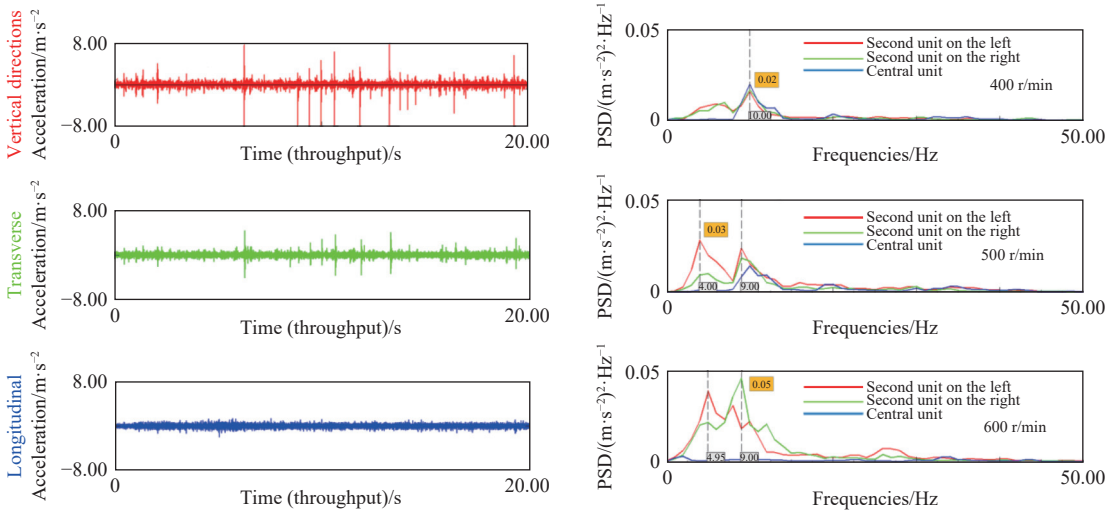

a. Time-domain signals in various directions for the central unit b. PSD of random longitudinal vibration signals

Figure 20 Random longitudinal vibration signals data processing

From the above figure, it can be observed that the longitudinal acceleration of the harvester exhibits a more significant amplitude variation. Therefore, the longitudinal vibration signals were considered as the primary vibration signals during harvester operation. Using the LMS Test Lab vibration-signal analysis software, the time-domain signals in the longitudinal direction at different speed levels and measurement points were processed. This included high/low (H/L) pass filtering, fast Fourier transform (FFT), and amplitude normalization after peak retention. The aim was to obtain the power spectral density (PSD) of the random vibration signals in the longitudinal direction for each measurement point at different operating speeds.

As shown in Figure 20b, when the seed-metering plate worked at speeds of 400, 500, and 600 r/min, the main excitation frequencies of the three measurement points were 10.00, 4.00, and 9.00 Hz, with peak PSD values of 0.02, 0.03, and 0.05 $(m/s^2)^2/Hz$,

respectively. It can be seen that as the harvester's forward speed increases, the amplitude peaks gradually rise. These data were used as the original data for indoor vibration-simulation testing.

For vibration-simulation testing, an E-03H06 hydraulic vibration test system from Suzhou STI Co., Ltd. was used. The control and analysis software corresponding to the vibration test bench was RC-3000-2, which controlled the PSD of the vibration signals and reproduced the vibration of multi-frequency composite signals. The control accuracy was within ±1 dB, allowing for an accurate simulation of the field working conditions. The indoor vibration test-bench setup is shown in Figure 21.

The PSD data obtained from the vibration signals processed by the analysis software described in Section 4.3.1 were imported into the vibration test-bench analysis software. This allowed the test bench to replicate the vibration environment during field operation at speeds ranging from 400 to 1000 r/min. With all other factors held constant, the working speed served as the influencing factor, and the seed-leakage rate was the primary impact indicator. The working effects of the four seed-metering plates from Section 4.4.1 were compared to verify the working performance of the proposed seed-metering device. Each test was repeated three times, with seed counts totaling 1000 seeds per test. The results are shown in Figure 22.

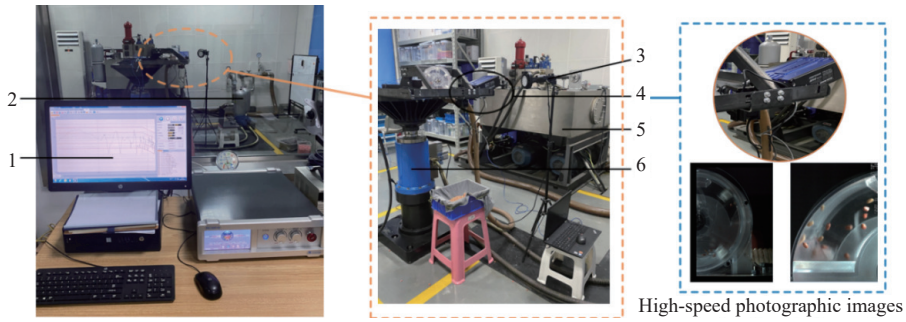

Figure 21 Indoor vibration-environment test setup

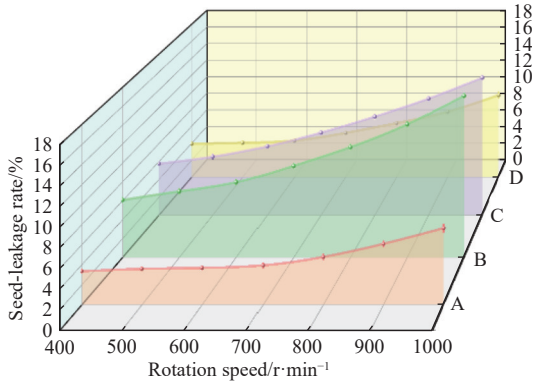

Figure 22 Vibration-simulation test results

From the figure, it can be seen that, compared to the static bench tests, the seed-leakage rate for all seed-metering plates increased under vibration conditions, indicating a decrease in seed-filling performance. When comparing the working effects of seed-metering plates *A* and *B* before and after optimization, it becomes evident that the seed-leakage rate of seed-metering plate *B* is consistently higher than that of *A* at different speed levels. Starting from 600 r/min, seed-metering plates *A* and *B* both exhibit a significant increase in the seed-leakage rate, with plate *B* showing a much larger variation. Seed-metering plates *B* and *C* have relatively high seed-leakage rate values, and when the speed exceeds 600 r/min, both show a clear upward trend in the seed-leakage rate. Seed-metering plates *A* and *D* have smaller variations in seed-leakage rate compared to plates *B* and *C*.

Although there are numerical differences in seed-leakage rate between plates *A* and *D* in the static bench and vibration environments, their trends are similar, indicating the ability to enhance the seed-filling performance to some extent. Plate *A* demonstrates superior performance. Therefore, it can be concluded that plate *A* is better suited to meet the seed-filling requirements under complex operational conditions.

4.4.3 Discussion of the validation-model results

The above experiments revealed that increasing the nozzle-orifice diameter and seed-filling-space angle both contribute to improved seed-filling performance. Moreover, the enhancement in seed-filling performance, owing to the increase in nozzle-orifice diameter, surpasses that of the reducing seed-filling-space angle. Therefore, it can be inferred that enlarging the nozzle-orifice diameter is the fundamental approach to enhancing the filling performance and seed-carrying stability, which aligns with the conclusions drawn from the simulations in Section 4.2.

Under the influence of pneumatic forces, seeds tend to move towards the nozzle. As the rotational speed increases, the time the seeds spend in the seed-filling area decreases, leading to an increase in the seed-leakage rate. For instance, in the static bench test (Section 4.4.1), when the working speed increased from 600 r/min to 700 r/min, the seed-leakage rate for seed-metering plate *B* increased from 6.45% to 7.88%, while for seed-metering plate *C*, which had a reduced seed-filling-space angle, the seed-leakage rate increased from 6.22% to 7.49%. It can be observed that both the absolute change and the numerical values of the seed-leakage rate for plate *C* are lower than those for plate *B* at the same speed level, suggesting that increasing the seed-filling-space angle can mitigate this adverse effect.

Once the target seeds enter the nozzle, they experience complex forces from the surrounding seed population. Under high-speed vibrational conditions, there is an increased probability of seeds dislodging from the nozzle, making seed leakage more likely. The presence of orifices at the nozzle provides some adhesion force to the target seeds. For example, in the vibration test results (Section 4.4.2), when the working speed increased from 600 r/min to 700 r/min under vibration conditions, the seed-leakage rate for seed-metering plate *B* increased from 7.98% to 9.7%, whereas for seed-metering plate *C* with varying nozzle-orifice diameters, the seed-leakage rate increased from 4.32% to 5.22%.

It is clear that under vibration conditions, with an increase in working speed, the seed-leakage rate for seed-metering plates *B* and *C* rapidly rises, while the increase in seed-leakage rate for plates *A* and *D* is relatively small. Therefore, increasing the nozzle-orifice diameter can counteract the adverse effects of high-speed and

vibrational environments, enhancing the seed-filling performance and seed-carrying stability.

5 Conclusions

This study employed a DEM-CFD coupled-analysis approach to simulate the effects of the nozzle-orifice diameter, seed-filling-space angle, and rotational speed on seed-motion characteristics. The DEM-CFD coupled model effectively described the seed-filling performance and seed-carrying stability of the seed-metering device during its operation. The main conclusions are as follows:

(1) The wheat seed-metering device operation process was analyzed, elucidating the working principles of the seed-filling and seed-cleaning processes and determining key structural parameters. The influencing factors on the seed-filling performance and seed-carrying stability were investigated, a combined mechanical-pneumatic seed-filling method was proposed, and the optimized target parameters were determined to be the nozzle-orifice diameter, seed-filling-space angle, and rotational speed.

(2) Based on the gas–solid coupled simulation results, the seed-filling and seed-carrying processes were evaluated and analyzed from both macroscopic and microscopic perspectives. Microscopically, the seed void fraction, resistance to clearing, and initial dropping position were defined as evaluation metrics, and single-factor experiments were conducted to obtain the influence trends and optimal ranges of each factor. The results indicated that with an increase in the nozzle-orifice diameter and seed-filling-space angle, the changes in the nozzle void fraction became smaller, and the values of the resistance to clearing increased. This suggests that the structural optimizations could effectively enhance the seed-filling performance and seed-carrying stability, with the nozzle-orifice diameter having a greater impact than the seed-filling-space angle. On a macroscopic scale, the seed-leakage rate, reseeding rate, and grain-spacing qualification rate were defined as evaluation metrics for orthogonal experiments. The results revealed the order of impact for the evaluation metrics and their interaction effects. Through secondary optimization experiments, the optimal parameter combinations for nozzle-orifice diameter, seed-filling-space angle, and rotational speed were determined as 1.7 mm, 39.3°, and 657.4 r/min, respectively.

(3) Static bench-validation tests were conducted. When the rotational speed of the seed-metering plate varied within the range of 400-1000 r/min, the seed-leakage rate for the optimized structure seed-metering plate was below 6.6%, and the reseeding rate was below 7.85%. All performance indices outperformed the original seed-metering plate. These demonstrate the effectiveness of the structural optimization in improving the seed-filling performance and seed-carrying stability.

(4) Vibration signals were acquired and analyzed under different working speeds during field seeding operations. Based on these data, indoor vibration-environment simulation experiments of the seed-metering device were conducted. The test results showed that the seed-leakage rate for the optimized-structure seed-metering plate was below 7.6%. All performance indices significantly outperformed the original seed-metering plate, indicating a substantial improvement in the seed-filling efficiency and seed-carrying stability.

By employing DEM-CFD coupled simulations to model the impact of pneumatic forces on seed-motion characteristics in the seed-metering device, this study explored the influence of different structural parameters on the seed-metering device's operational performance. The model was verified to be reliable and effective.

Acknowledgements

This work was supported by the Key R&D Program of Shandong Province, China (Grant No. 2024CXGC010901), Shandong Academy of Agricultural Sciences Unveils Marshal Program (Grant No. SHJB2021-94), and Shandong Academy of Agricultural Sciences and Technology Innovation Project (Grant No. CXGC2025C16).

[References]

[1] Zhai J B, Xia J F, Zhou Y, Zhang S. Design and experimental study of the control system for precision seed-metering device. Int J Agric & Biol Eng, 2014; 7(3): 13–18.

[2] Lei X L, Hu H J, Yang W H, Liu L Y, Liao Q X, Ren W J. Seeding performance of air-assisted centralized seed-metering device for rapeseed. Int J Agric & Biol Eng, 2021; 14(5): 79–87.

[3] Manzone M, Paolo M, Mario T, Balsari P. Performance evaluation of a cyclone to clean the air exiting from pneumatic seed drills during maize sowing. Crop Protection, 2015; 76: 33–38.

[4] Bourges G, Medina M. Air-seeds flow analysis in a distributor head of an "air drill" seeder. Acta Hortic, 2013; 1008: 259–264.

[5] Lei X L, Liao Y T, Li Z D, Cao X Y, Li S S, Wei Y P, et al. Design and experiment of seed feeding device in air-assisted centralized metering device for rapeseed and wheat. Transactions of the CSAE, 2015; 31(20): 10–18.

[6] Zhang G Z, Zang Y, Luo X W, Wang Z M, Li Z D. Line-churning tooth design and metering accuracy experiment of rice pneumatic precision hill-drop seed metering device on pregnant Japonica rice seed. Transactions of the CSAE, 2014; 30(17): 1–9.

[7] He S Y, Qian C, Jiang Y C, Qin W, Huang Z S, Huang D M, et al. Design and optimization of the seed feeding device with DEM-CFD coupling approach for rice and wheat. Computers and Electronics in Agriculture, 2024; 219: 0168–1699.

[8] Shi S, Zhou J L, Liu H, Fang H M, Jian S C, Zhang R F. Design and experiment of pneumatic precision seed-metering device with guided assistant seed-filling. Transactions of the CSAM, 2019; 50(5): 61–70. DOI: 10.6041 //j.issn.1000-1298.2019.05.007. (in Chinese)

[9] Li H, Liu H, Zhou J L, Wei G J, Shi S, Zhang X C, et al. Development and first results of a no-till pneumatic seeder for maize precise sowing in Huang-Huai-Hai Plain of China. Agriculture, 2021; 11(10): 1023.

[10] Hu H J, Zhou Z L, Wu W C, Yang W H, Li T, Chang C, et al. Distribution characteristics and parameter optimisation of an air-assisted centralised seed-metering device for rapeseed using a CFD-DEM coupled simulation. Biosystems Engineering, 2021; 208: 246–259.

[11] Ren B, Zhong W Q, Chen Y, Chen X, Jin B S, Yuan Z L, et al. CFD-DEM simulation of spouting of corn-shaped particles. Particuology, 2012; 10(5): 562–572.

[12] Tong Z B, Zheng B, Yang R Y, Yu A B, Chan H K. CFD-DEM investigation of the dispersion mechanisms in commercial dry powder inhalers. Powder Technol, 2013; 240: 19–24.

[13] Akhshik S, Behzad M, Rajabi M. CFD–DEM approach to investigate the effect of drill pipe rotation on cuttings transport behavior. Journal of Petroleum Science and Engineering, 2015; 127: 229–244.

[14] Krause B, Liedmann B, Wiese J, Wirtz S, Scherer V. Coupled three dimensional DEM–CFD simulation of a lime shaft kiln—Calcination, particle movement and gas phase flow field. Chemical Engineering Science, 2015; 134: 834–849.

[15] Iqbal N, Rauh C. Coupling of discrete element model (DEM) with computational fluid mechanics (CFD): A validation study. Applied Mathematics and Computation, 2016; 277: 154–163.

[16] Brosh T, Kalman H, Levy A, Peyron I, Ricard F. DEM-CFD simulation of particle comminution in jet-mill. Powder Technology, 2014; 257: 104–112.

[17] Zhou H, Mo G Y, Zhao J P, Cen K. DEM–CFD simulation of the particle dispersion in a gas–solid two-phase flow for a fuel-rich/lean burner. Fuel, 2011; 90(4): 1584–1590.

[18] Liu M L, Wen Y Y, Liu R Z, Liu B, Shao Y L. Investigation of fluidization behavior of high density particle in spouted bed using CFD–DEM coupling method. Powder Technology, 2015; 280: 72–82.

[19] Lei X L, Liao Y T, Liao Q X. Simulation of seed motion in seed feeding device with DEM-CFD coupling approach for rapeseed and wheat. Computers and Electronics in Agriculture, 2016; 131: 29–39.

[20] Wang Y B, Li H W, Hu H N, He J, Wang Q J, Lu C Y, et al. DEM-CFD coupling simulation and optimization of a self-suction wheat shooting device. Powder Technology, 2021; 393: 494–509.

[21] Zhao X S, Hou Z Z, Lyu W, Lu C, Yu H L, Wei Z M. Design and test of a positive-negative pressure quinoa precision seed-metering device with a disturbed seed-filling mechanism. Int J Agric & Biol Eng, 2024; 17(6): 121–134.

[22] Han D D, Zhang D X, Jing H R, Yang L, Cui T, Ding Y Q, et al. DEM-CFD coupling simulation and optimization of an inside-filling air-blowing maize precision seed-metering device. Computers and Electronics in Agriculture, 2018; 150: 426–438.

[23] Wang Y B, Li H W, Hu H N, He J, Wang Q J, Lu C Y, et al. A noncontact self-suction wheat shooting device for sustainable agriculture: A preliminary research. Computers and Electronics in Agriculture, 2020; 197: 106927.

[24] Sun X P, Li H, Qi X D, Feng D H, Zhou J Q, Wang Y J, et al. Optimization of a three-row air-suction Brassica chinensis precision metering device based on CFD-DEM coupling simulation. Int J Agric & Biol Eng, 2023; 16(3): 130–142.

[25] Zhao X S, Bai W J, Li J, Yu H L, Zhao D W, Yin B Z. Study on positive-negative pressure seed metering device for wide-seedling-strip-seeding. Int J Agric & Biol Eng, 2022; 15(6): 124–133.

[26] Xu H M, Liu W R, Liu H, Liu Z F, Zhang G Z. Design and performance test of a combined and adjustable precise rice seed metering device. Int J Agric & Biol Eng, 2025; 18(1): 101–114.

[27] Wang Y B, He M Z, Yan Q H, Zheng Z W. DEM-CFD simulation and seed orientation evaluation of a self-suction wheat shooting device. Powder Technology, 2023; 427: 118746.

[28] Lai Q H, Sun K, Yu Q X, Qin W. Design and experiment of a six-row air-blowing centralized precision seed-metering device for Panax notoginseng. Int J Agric & Biol Eng, 2020; 13(2): 111–122.

[29] Zhang Z, Xie Z L. Numerical simulation of fluid-solid two-phase flows. Journal of Chemical Industry and Engineering, 2001; 52(1): 1–12.

[30] Shi S, Liu H, Wei G J, Zhou J L, Jian S C, Zhang R F. Optimization and experiment of pneumatic seed metering device with guided assistant filling based on EDEM-CFD. Transactions of the CSAM, 2020; 51(5): 54–66. DOI: 10.6041 /j.issn: 1000–1298.2020.05.006. (in Chinese)